**Group 10**

Full Name	Student ID
Ehsan Lakzaei	1261797
Gregorius R. Widojoko	1773828

Lecturer: Prof. dr. Siep Weiland

1 | Problem Formulation

This report discusses the analysis of temperature distribution on a locally heated surface. In particular, lithography machines with Extreme Ultra Violet (EUV) sources are in our interest. These machines are used to produce microchips in large scales. There are different source of errors that can influence the performance of these machines and consequently the quality of the wafer that contains the microchips. Among these errors, the supplied heat of the light source may cause deformation of the wafer thermally and needs to be compensated. The given model is described with a Partial Differential Equation (PDE) as following:

$$\rho(x, y)c(x, y)\frac{\partial T}{\partial t}(x, y, t) = \left[\begin{array}{cc} \frac{\partial}{\partial x} & \frac{\partial}{\partial y} \end{array} \right] K(x, y) \left[\begin{array}{c} \frac{\partial T(x, y)}{\partial x} \\ \frac{\partial T(x, y)}{\partial y} \end{array} \right] + u(x, y, t) \quad (1)$$

Through the project, authors start analysing the property of the system 1, then assuming homogeneity of the model the solution of system is found with help of separation of variables. Afterwards, the orthonormality of the basis function, Galerkin projection and steady state solution are discussed. Lastly, the results of simulation with different settings are shown.

2 | Properties of the model

2.1 | Linearity, Time Variance and Homogeneity

In this section, the linearity of the model, presented in equation 1, is discussed and proved. Next, it is illustrated why the model is time-invariant and lastly the cases where the model is homogeneous and non-homogeneous are presented.

Linearity:

A system is linear when the linear combination of the solution is a solution. Therefore, if (u, T) considered a solution to system 1, so is $(2u, 2T)$ a solution. Filling this solution in equation 1 leads to:

$$\begin{aligned} \rho c \frac{\partial 2T}{\partial t}(x, y, t) &= \left[\begin{array}{cc} \frac{\partial}{\partial x} & \frac{\partial}{\partial y} \end{array} \right] K \left[\begin{array}{c} \frac{\partial 2T(x, y)}{\partial x} \\ \frac{\partial 2T(x, y)}{\partial y} \end{array} \right] + 2u(x, y, t) = \\ 2 \left[\begin{array}{cc} \frac{\partial}{\partial x} & \frac{\partial}{\partial y} \end{array} \right] K(x, y) \left[\begin{array}{c} \frac{\partial T(x, y)}{\partial x} \\ \frac{\partial T(x, y)}{\partial y} \end{array} \right] &+ 2u(x, y, t) \end{aligned}$$

It is clear from equation above that the pair $(2u, 2T)$ is also a solution and hence the model is linear, considering the model being an isotropic model which leads to K be constant.

Time-invariant:

A system is time-invariant if and only if applying a time shift in the input results the same time shift in the output. Considering this time shift and applying it to system represented in 1 leads to:

$$\rho(x, y)c(x, y)\frac{\partial T}{\partial t}(x, y, t + \tau) = \left[\begin{array}{cc} \frac{\partial}{\partial x} & \frac{\partial}{\partial y} \end{array} \right] K(x, y) \left[\begin{array}{c} \frac{\partial T(x, y)}{\partial x} \\ \frac{\partial T(x, y)}{\partial y} \end{array} \right] + u(x, y, t + \tau) \quad (2)$$

One can conclude that equations 1 and 2 are the same with a τ shift in time in equation 2. Therefore, the system is time invariant.

Homogeneous and non-homogeneous:

The represented model for heat diffusion phenomenon is characterized by its first partial derivative with respect to time (t) and its second partial derivative with respect to the spatial variables (x, y) . One can write the non-homogeneous equation 1 in terms of the linear heat as following:

$$\mathcal{L}(T) = \frac{1}{\rho(x, y)c(x, y)} \cdot u(x, y, t)$$

*Note: this is possible since material density and heat capacity are both uniform and constant assumed. Where the diffusion operator in two spatial variables reads:

$$\mathcal{L}(T) = \rho(x, y)c(x, y)\frac{\partial T}{\partial t}(x, y, t) - \left[\begin{array}{cc} \frac{\partial}{\partial x} & \frac{\partial}{\partial y} \end{array} \right] K(x, y) \left[\begin{array}{c} \frac{\partial T(x, y)}{\partial x} \\ \frac{\partial T(x, y)}{\partial y} \end{array} \right]$$

When there is no heat generation, then $u(x, y, t) = 0$ and hence, the non-homogeneous partial differential equation reduces to its corresponding homogeneous:

$$\begin{aligned}\mathcal{L}(T) = 0 \rightarrow \rho(x, y)c(x, y)\frac{\partial T}{\partial t}(x, y, t) &= \left[\frac{\partial}{\partial x} \quad \frac{\partial}{\partial y} \right] K(x, y) \begin{bmatrix} \frac{\partial T(x, y)}{\partial x} \\ \frac{\partial T(x, y)}{\partial y} \end{bmatrix} \\ \frac{\partial T}{\partial t}(x, y, t) &= \frac{k}{\rho(x, y) \cdot c(x, y)} \cdot (T_{xx} + T_{yy})\end{aligned}$$

Where $\frac{k}{\rho(x, y) \cdot c(x, y)}$ is called thermal diffusivity and is constant, positive and uniform (based on the given specification in project description).

3 | The homogeneous model

3.1 | Question 2

From this point forward (until further notice), it is assumed that the model is homogeneous and the following is valid:

$$\ell_x = \ell_y = 0$$

and let $\rho(x, y) = \rho$, $c(x, y) = c$ and $\kappa(x, y) = \kappa$ be positive constants.

In this section, it will be shown that under these conditions, system 1 admits the following solution:

$$T(x, y, t) = a(t)\varphi^{(x)}(x)\varphi^{(y)}(y) = T(t)X(x)Y(y) \quad (3)$$

Where a , $\varphi^{(x)}$ and $\varphi^{(y)}$ are scalar-valued functions on \mathbb{R} , $[0, L_x]$ and $[0, L_y]$, respectively which satisfies:

$$\ddot{\varphi}^{(x)} - \lambda_x \varphi^{(x)} = 0, \quad \ddot{\varphi}^{(y)} - \lambda_y \varphi^{(y)} = 0, \quad \dot{a} - \lambda a = 0$$

In order to prove this, system 1 will be re-written in a compact form under conditions mentioned above, as following:

$$T_t = \frac{\kappa}{\rho c}[T_{xx} + T_{yy}] \quad (4)$$

Filling the admitted solution 3 in equation 4 will lead to:

$$\begin{aligned}X(x)Y(y)\frac{d}{dt}T(t) &= \frac{\kappa}{\rho c}(\frac{d^2}{dx^2}X(x)Y(y)T(t) + \frac{d^2}{dy^2}Y(y)X(x)T(t)) \\ \frac{\rho c}{\kappa} \frac{\dot{T}}{T(t)} &= \frac{\frac{d^2}{dx^2}X(x)}{X(x)} + \frac{\frac{d^2}{dy^2}Y(y)}{Y(y)}\end{aligned} \quad (5)$$

Left hand side of equation 5 is an exclusive function of t and the right hand side is an exclusive function of x and y . Since x , y and t are independent from each other, equation 5 holds if and only if both sides are constants. We set each terms equal to a constant (separation constant) $\lambda^2 \in \mathbb{R}$ and make it negative for convenience later, which leads to the following equations:

$$\begin{aligned}\dot{T} &= -\frac{\kappa}{\rho c}\lambda^2 T(t) \\ \ddot{X}(x) &= -\lambda_x^2 X(x) \\ \ddot{Y}(y) &= -\lambda_y^2 Y(y) \\ \lambda^2 &= \lambda_x^2 + \lambda_y^2\end{aligned} \quad (6)$$

One can solve these Ordinary Differential Equations (ODEs) in 6 as following:

$$\ddot{X}(x) + \lambda_x^2 X(x) = 0 \quad (7)$$

Since equation 7 can be considered as: $r^2 + \lambda_x^2 \cdot r = 0 \rightarrow D < 0$, equation 7 has a solution of the form: $X(x) = C_1 \cdot \sin(\lambda_x x) + C_2 \cdot \cos(\lambda_x x)$ at which the first derivative can be computed as:

$$\dot{X}(x) = \lambda_x \cdot (C_1 \cdot \cos(\lambda_x x) - C_2 \cdot \sin(\lambda_x x))$$

Considering the boundary conditions that are described in the project description:

$$\dot{X}(0) = 0 \rightarrow C_1 = 0$$

and

$$\dot{X}(L_x) = 0 \rightarrow \lambda_x L_x = K \cdot \pi, \quad K \in \mathbb{Z}, \text{ hence: } \lambda_x = \frac{K \cdot \pi}{L_x}, \quad K = 0, 1, 2, \dots$$

Which can be substituted in the solution form and thus:

$$X(x) = C_2 \cdot \cos\left(\frac{K \cdot \pi}{L_x} x\right), \quad K = 0, 1, 2, \dots \quad (8)$$

Applying the same principle for $\ddot{Y}(y) + \lambda_y^2 Y(y) = 0$ leads to:

Form of solution: $Y(y) = C_3 \cdot \sin(\lambda_y y) + C_4 \cdot \cos(\lambda_y y)$ where the first derivative is:

$$\dot{Y}(y) = \lambda_y \cdot (C_3 \cdot \cos(\lambda_y y) - C_4 \cdot \sin(\lambda_y y))$$

Considering the given boundary conditions:

$$\dot{Y}(0) = 0 \rightarrow C_3 = 0$$

and

$$\dot{Y}(L_y) = 0 \rightarrow \lambda_y L_y = \ell \cdot \pi, \ell \in \mathbb{Z}, \text{ hence: } \lambda_y = \frac{\ell \cdot \pi}{L_y}, \ell = 0, 1, 2, \dots$$

Thus:

$$Y(y) = C_4 \cdot \cos\left(\frac{\ell \cdot \pi}{L_y} y\right), \quad \ell = 0, 1, 2, \dots \quad (9)$$

Lastly, $\dot{T} + \frac{\kappa}{\rho c} \lambda^2 T(t) = 0$ has a solution from:

$$T(t) = C_5 \cdot e^{-\frac{\kappa}{\rho c} \lambda t} = C_5 \cdot e^{-(\lambda_x + \lambda_y)t} \quad (10)$$

Based on equations 8, 9 and 10, one can observe that system 1 admits the solution:

$$T(x, y, t) = a(t) \varphi^{(x)}(x) \varphi^{(y)}(y) = T(t) X(x) Y(y)$$

where $T(t)$, $X(x)$ and $Y(y)$ satisfies equations set 6 under conditions:

$\ell_x = \ell_y = 0$, $\rho(x, y) = \rho$, $c(x, y) = c$ and $\kappa(x, y) = \kappa$.

3.2 | Question 3

In this part, the orthonormality of the set $\{\varphi_{k,\ell} \mid 0 \leq k \leq K, 0 \leq \ell \leq L\}$ for any $K > 0$ and $L > 0$ to the set of functions in \mathcal{L}_2 will be illustrated, where the set \mathcal{L}_2 defines the inner product space of all functions with the standard inner product:

$$\mathcal{L}_2 := \langle \varphi_i, \varphi_j \rangle := \int_0^{L_x} \int_0^{L_y} \varphi_i(x, y) \cdot \varphi_j(x, y) dy dx. \quad (11)$$

Furthermore, a spectral decomposition of the temperature evolution is proposed:

$$T(x, y, t) = \sum_{k=0}^{\infty} \sum_{\ell=0}^{\infty} a_{k,\ell}(t) \cdot \varphi_k^{(x)} \cdot \varphi_{\ell}^{(y)} \quad (12)$$

where, for non-negative integers k and ℓ :

$$\varphi^{(x)}(x) = \begin{cases} \left(\frac{1}{\sqrt{L_x}}\right) & \text{if } k = 0 \\ \left(\sqrt{\frac{2}{L_x}}\right) \cdot \cos\left(\frac{k\pi x}{L_x}\right) & \text{if } k > 0 \end{cases} \quad \varphi^{(y)}(y) = \begin{cases} \left(\frac{1}{\sqrt{L_y}}\right) & \text{if } \ell = 0 \\ \left(\sqrt{\frac{2}{L_y}}\right) \cdot \cos\left(\frac{\ell\pi y}{L_y}\right) & \text{if } \ell > 0 \end{cases} \quad (13)$$

and $a_{k,\ell}(t)$ is a double-indexed time-varying coefficient. Moreover,

$$\varphi_{k,\ell}(x, y) := \varphi_k^{(x)}(x) \cdot \varphi_{\ell}^{(y)}(y)$$

where $x \in [0, L_x]$ and $y \in [0, L_y]$. Then $\{\varphi_{k,\ell} \mid k, \ell = 0, 1, 2, \dots\}$ denotes an infinite collection of functions that are square integrable on $[0, L_x] \times [0, L_y]$.

A set of functions $\{\phi_m(t) \mid m = 0, 1, 2, \dots\}$ are said to be orthogonal over the interval $[t_0, t_f]$ if:

$$\int_{t_0}^{t_f} \phi_m(t) \cdot \phi_r(t) dt = \begin{cases} 0 & \text{when } m \neq r \\ c & \text{when } m = r \end{cases}$$

when c is a non-zero positive constant. When $c = 1$, the set $\{\phi_m(t)\}$ is known as orthonormal set over the interval. Based on this definition, if one plugs equations 13 in equation 11 will obtain:

$$\langle \varphi_i, \varphi_j \rangle := \int_0^{L_x} \int_0^{L_y} \varphi_i(x, y) \cdot \varphi_j(x, y) dy dx$$

$$\int_0^{L_x} \left(\sqrt{\frac{2}{L_x}} \right)^2 \cdot \cos\left(\frac{k\pi}{L_x}x\right) \cdot \cos\left(\frac{\ell\pi}{L_x}x\right) dx \cdot \int_0^{L_y} \left(\sqrt{\frac{2}{L_y}} \right)^2 \cdot \cos\left(\frac{k\pi}{L_y}y\right) \cdot \cos\left(\frac{\ell\pi}{L_y}y\right) dy \\ \int_0^{L_x} \left(\frac{1}{L_x} \right) \cdot \left[\cos\left(\frac{(k+\ell)\pi x}{L_x}\right) + \cos\left(\frac{(k-\ell)\pi x}{L_x}\right) \right] dx \cdot \int_0^{L_y} \left(\frac{1}{L_y} \right) \cdot \left[\cos\left(\frac{(k+\ell)\pi y}{L_y}\right) + \cos\left(\frac{(k-\ell)\pi y}{L_y}\right) \right] dy$$

when $k \neq \ell$ the integral above leads to:

$$= \frac{1}{L_x} \left[\left(\frac{L_x}{(k+\ell)\pi} \right) \cdot \sin\left(\frac{(k+\ell)\pi}{L_x}x\right) + \left(\frac{L_x}{(k-\ell)\pi} \right) \cdot \sin\left(\frac{(k-\ell)\pi}{L_x}x\right) \right]_0^{L_x} \times \\ \frac{1}{L_y} \left[\left(\frac{L_y}{(k+\ell)\pi} \right) \cdot \sin\left(\frac{(k+\ell)\pi}{L_y}y\right) + \left(\frac{L_y}{(k-\ell)\pi} \right) \cdot \sin\left(\frac{(k-\ell)\pi}{L_y}y\right) \right]_0^{L_y} \\ = \frac{1}{(k+\ell)\pi} \cdot \sin((k+\ell)\pi) + \frac{1}{(k-\ell)\pi} \cdot \sin((k-\ell)\pi) \times \\ \frac{1}{(k+\ell)\pi} \cdot \sin((k+\ell)\pi) + \frac{1}{(k-\ell)\pi} \cdot \sin((k-\ell)\pi) = 0$$

since, "sin(integer · π) = 0".

When $k = \ell$ the integral above leads to:

$$\int_0^{L_x} \left(\frac{1}{L_x} \right) \cdot \left[\cos\left(\frac{(k+\ell)\pi x}{L_x}\right) + 1 \right] dx \cdot \int_0^{L_y} \left(\frac{1}{L_y} \right) \cdot \left[\cos\left(\frac{(k+\ell)\pi y}{L_y}\right) + 1 \right] dy \\ = \frac{1}{L_x} \cdot \left[\frac{L_x}{(k+\ell)\pi} \cdot \sin((k+\ell)\pi) + L_x \right] \cdot \frac{1}{L_y} \cdot \left[\frac{L_y}{(k+\ell)\pi} \cdot \sin((k+\ell)\pi) + L_y \right] = 1 \cdot 1 = 1$$

Therefore, based on the definition of orthonormality mentioned above, the set $\{\varphi_{k,\ell} | 0 \leq k \leq K, 0 \leq \ell \leq L\}$ for any $K > 0$ and $L > 0$ is orthonormal to the set of functions in \mathcal{L}_2 .

3.3 | Question 4

In this section, first the Galerkin projection is applied to derive an explicit ODE for the coefficient function $a_{k,\ell}(t)$ in the spectral expansion 12 for arbitrary k and ℓ . Then, the equilibrium solution will be determined when there is no heat generation (in other words: $u_1(t) = u_2(t) = 0$).

3.3.1 | Galerkin Projection

Under conditions mentioned in 3.1, system equation becomes:

$$\rho c \frac{\partial T}{\partial t} - \kappa \left(\frac{\partial^2 T}{\partial x^2} + \frac{\partial^2 T}{\partial y^2} \right) - u = 0. \quad (14)$$

Considering basis function $\varphi_n, n = 0, 1, 2, \dots$ such that:

$$\langle \varphi_n, \varphi_{k,\ell}(x, y) \rangle = \begin{cases} 0 & \text{if } (k, \ell) \neq n \\ 1 & \text{if } (k, \ell) = n \end{cases}$$

where,

$$\varphi_{k,\ell}(x, y) := \varphi_k^{(x)}(x) \cdot \varphi_\ell^{(y)}(y).$$

One can apply the inner product between system equation 14 and basis function which is as following:

$$\langle \varphi_n, \rho c \frac{\partial T}{\partial t} - \kappa \left(\frac{\partial^2 T}{\partial x^2} + \frac{\partial^2 T}{\partial y^2} \right) - u \rangle = 0, \quad n = 1, 2, \dots$$

Considering the superposition rule for the inner product:

$$\langle \varphi_n, \rho c \frac{\partial T}{\partial t} \rangle - \left\langle \varphi_n, \kappa \left(\frac{\partial^2 T}{\partial x^2} + \frac{\partial^2 T}{\partial y^2} \right) \right\rangle - \langle \varphi_n, u \rangle = 0, \quad n = 1, 2, \dots$$

Plugging equation 12 in above equation results:

$$\left\langle \varphi_n, \rho c \frac{\partial \left(\sum_{k=0}^{\infty} \sum_{\ell=0}^{\infty} a_{k,\ell}(t) \cdot \varphi_{k,\ell}(x, y) \right)}{\partial t} \right\rangle$$

$$\begin{aligned}
& - \left\langle \varphi_n, \kappa \left(\frac{\partial^2 \left(\sum_{k=0}^{\infty} \sum_{\ell=0}^{\infty} a_{k,\ell}(t) \cdot \varphi_{k,\ell}(x, y) \right)}{\partial x^2} + \frac{\partial^2 \left(\sum_{k=0}^{\infty} \sum_{\ell=0}^{\infty} a_{k,\ell}(t) \cdot \varphi_{k,\ell}(x, y) \right)}{\partial y^2} \right) \right\rangle \\
& \quad - \left\langle \varphi_n, u \right\rangle = 0, \quad n = 1, 2, \dots
\end{aligned}$$

Eliminating partials and considering boundary conditions:

$$\begin{aligned}
& \left\langle \varphi_n, \rho c \left(\sum_{k=1}^{\infty} \sum_{\ell=1}^{\infty} a_{k,\ell}(t) \cdot \varphi_{k,\ell}(x, y) \right) \right\rangle \\
& - \left\langle \varphi_n, \kappa \left(\left(\sum_{k=1}^{\infty} \sum_{\ell=1}^{\infty} a_{k,\ell}(t) \cdot \ddot{\varphi}_{k,\ell}^{(x)}(x, y) \right) + \left(\sum_{k=1}^{\infty} \sum_{\ell=1}^{\infty} a_{k,\ell}(t) \cdot \ddot{\varphi}_{k,\ell}^{(y)}(x, y) \right) \right) \right\rangle \\
& \quad - \left\langle \varphi_n, u \right\rangle = 0, \quad n = 1, 2, \dots
\end{aligned}$$

Orthonormality property of the basis function leads to:

$$\rho c \dot{a}_n = \kappa \sum_{k=1}^r \sum_{\ell=1}^r a_{k,\ell}(t) \left(\left\langle \varphi_n, \ddot{\varphi}_{k,\ell}^{(x)}(x, y) \right\rangle + \left\langle \varphi_n, \ddot{\varphi}_{k,\ell}^{(y)}(x, y) \right\rangle \right) + \left\langle \varphi_n, u \right\rangle, \quad n = 1, 2, \dots, r \quad (15)$$

Using the second partial derivative with respect to x and y in equation sets 13:

$$\left\langle \varphi_n, \ddot{\varphi}_{k,\ell}^{(x)}(x, y) \right\rangle = \begin{cases} 0 & \text{when } k, \ell \neq n \\ -\left(\frac{n\pi}{L_x}\right)^2 & \text{when } k, \ell = n \end{cases}$$

and

$$\left\langle \varphi_n, \ddot{\varphi}_{k,\ell}^{(y)}(x, y) \right\rangle = \begin{cases} 0 & \text{when } k, \ell \neq n \\ -\left(\frac{n\pi}{L_y}\right)^2 & \text{when } k, \ell = n \end{cases}$$

one can simplify equation 15 by considering separation variables for the input $u(x, y, t) = s(x, y)v(t)$ as following:

$$\rho c \dot{a}_n = -\kappa\pi^2 n^2 \left(\frac{L_x^2 + L_y^2}{L_x^2 \cdot L_y^2} \right) a_n + \left\langle \varphi_n, s(x, y) \right\rangle v(t), \quad n = 1, 2, \dots, r \quad (16)$$

which can be represented with state space model of $\boxed{\dot{a}(t) = A \cdot a(t) + B \cdot v(t)}$, where

$$A = \frac{\kappa}{\rho c} \begin{bmatrix} -\pi^2 \frac{L_x^2 + L_y^2}{L_x^2 \cdot L_y^2} & 0 & \cdots & \cdots & 0 \\ 0 & -4\pi^2 \frac{L_x^2 + L_y^2}{L_x^2 \cdot L_y^2} & 0 & \cdots & \vdots \\ \vdots & 0 & \ddots & 0 & \vdots \\ \vdots & \vdots & 0 & \ddots & 0 \\ 0 & 0 & \cdots & 0 & -r^2 \pi^2 \frac{L_x^2 + L_y^2}{L_x^2 \cdot L_y^2} \end{bmatrix}, \quad B = \frac{1}{\rho c} \begin{bmatrix} \langle \varphi_1, s(x, y) \rangle \\ \vdots \\ \langle \varphi_r, s(x, y) \rangle \end{bmatrix}$$

3.3.2 | Equilibrium solution

In steady state (i.e. $\dot{T}(t) = 0$), one can use equation 5 to find the equilibrium solution:

$$\nabla^2 T(x, y) = 0 \rightarrow T_{xx} + T_{yy} = 0 \quad (17)$$

The surface is insulated (perfectly) at the boundaries in the sense that:

$$\frac{\partial T(x, y)}{\partial x} \Big|_{x=0, L_x} = 0 \quad \text{and} \quad \frac{\partial T(x, y)}{\partial y} \Big|_{y=0, L_y} = 0$$

where the initial temperature $T(x, y, 0) = f(x, y)$ is a smooth function. The boundary condition can be interpreted as: "the temperature can flow in all directions but none of it can escape through the edges". Equation 17 can be solved with help of separation variables:

$$T(x, y) = X(x) \cdot Y(y) \quad (18)$$

with:

$$\begin{aligned}\frac{\partial T(x, y)}{\partial x} &= X'Y \quad \text{and} \quad \frac{\partial^2 T(x, y)}{\partial x^2} = X''Y \\ \frac{\partial T(x, y)}{\partial y} &= Y'X \quad \text{and} \quad \frac{\partial^2 T(x, y)}{\partial y^2} = Y''X\end{aligned}$$

Plugging these second partial derivatives in equation 17 and using separation constant: $-\lambda$, leads to:

$$\frac{X''}{X} = -\frac{Y''}{Y} = -\lambda$$

and hence:

$$X'' + \lambda X = 0 \quad \text{with boundary condition} \quad \left. \frac{\partial T(x, y)}{\partial x} \right|_{x=0, L_x} = 0 \quad (19)$$

$$Y'' - \lambda Y = 0 \quad \text{with boundary condition} \quad \left. \frac{\partial T(x, y)}{\partial y} \right|_{y=0, L_y} = 0 \quad (20)$$

There are three cases for each one of equations 19 and 20 with respect to choosing different values for λ , namely: $\lambda = -\alpha^2$, $\lambda = 0$ and $\lambda = \alpha^2$. Starting with equation 19:

■ case 1:

$$X'' + \lambda X = 0 \xrightarrow{\lambda = -\alpha^2} X'' - \alpha^2 X = 0$$

which has a solution form of: $X(x) = C_1 \cdot e^{\alpha \cdot x} + C_2 \cdot e^{-\alpha \cdot x}$. Considering the second partial derivatives of this solution and boundary conditions, this case leads to trivial solution: $C_1 = 0$ and $C_2 = 0$.

■ case 2:

$$X'' + \lambda X = 0 \xrightarrow{\lambda = 0} X'' = 0$$

which has a solution form of: $X(x) = C_3 \cdot x + C_4$. Considering the second partial derivatives of this solution and boundary conditions, this case leads to a solution: $X(x) = C_4$.

■ case 3:

$$X'' + \lambda X = 0 \xrightarrow{\lambda = \alpha^2} X'' + \alpha^2 X = 0$$

which has a solution form of: $X(x) = C_5 \cdot \sin(\alpha x) + C_6 \cdot \cos(\alpha x)$. Considering the second partial derivatives of this solution and boundary conditions, this case leads to a solution: $X(x) = C_6 \cdot \cos(\frac{n\pi}{L_x} x)$.

Moving to next step which is equation 20 and analysing the cases:

■ case 1:

$$Y'' - \lambda Y = 0 \xrightarrow{\lambda = -\alpha^2} Y'' + \alpha^2 Y = 0$$

which has a solution form of: $Y(y) = C_7 \cdot \sin(\alpha y) + C_8 \cdot \cos(\alpha y)$. Considering the second partial derivatives of this solution and boundary conditions, this case leads to a solution: $Y(y) = C_8 \cdot \cos(\frac{n\pi}{L_y} y)$.

■ case 2:

$$Y'' - \lambda Y = 0 \xrightarrow{\lambda = 0} Y'' = 0$$

which has a solution form of: $Y(y) = C_9 \cdot y + C_{10}$. Considering the second partial derivatives of this solution and boundary conditions, this case leads to a solution: $Y(y) = C_{10}$.

■ case 3:

$$Y'' - \lambda Y = 0 \xrightarrow{\lambda = \alpha^2} Y'' - \alpha^2 Y = 0$$

which has a solution form of: $Y(y) = C_{11} \cdot e^{\alpha \cdot y} + C_{12} \cdot e^{-\alpha \cdot y}$. Considering the second partial derivatives of this solution and boundary conditions, this case leads to trivial solution: $C_{11} = 0$ and $C_{12} = 0$.

Using these solutions (filling them in 18) and superposition property will lead to:

$$\begin{aligned}T(x, y) &= X(x) \cdot Y(y) = 0 \cdot \left(\sum_{n=1}^{\infty} C_8 \cdot \cos\left(\frac{n\pi}{L_y} y\right) \right) + C_4 \cdot C_{10} + \left(\sum_{n=1}^{\infty} C_6 \cdot \cos\left(\frac{n\pi}{L_x} x\right) \right) \cdot 0 \\ &= C_4 \cdot C_{10} = A_{00}\end{aligned} \quad (21)$$

Equation 21 shows that in steady state the temperature is constant which can be found by using Fourier series as following (considering smoothness of $f(x, y)$ and the domain $[0, L_x] \times [0, L_y]$):

$$\begin{aligned}T(x, y, 0) &= f(x, y) = \sum_{n=0}^{\infty} \sum_{m=0}^{\infty} A_{m,n} \sin\left(\frac{m\pi}{L_x} x\right) \cdot \sin\left(\frac{n\pi}{L_y} y\right) \\ A_{m,n} &= \frac{4}{L_x \cdot L_y} \int_0^{L_x} \int_0^{L_y} f(x, y) \cdot \sin\left(\frac{m\pi}{L_x} x\right) \cdot \sin\left(\frac{n\pi}{L_y} y\right) dy dx\end{aligned} \quad (22)$$

3.4 | Question 5 and 6

In order to simulate system 14 with $u = 0$ and the truncated expansion:

$$T_{K,L}(x,y,t) = \sum_{k=0}^K \sum_{\ell=0}^L a_{k,\ell}(t) \varphi_{k,\ell}(x,y) \quad K > 0, L > 0$$

one can apply finite difference method. To do so, the time derivative is replaced with first order forward-difference and the spatial derivative is replaced by a second order centred-difference approximation:

$$\frac{T_{i,j}^{n+1} - T_{i,j}^n}{\Delta t} = \frac{\kappa}{\rho c} \cdot \left(\left[\frac{T_{i-1,j}^n - 2 \cdot T_{i,j}^n + T_{i+1,j}^n}{\Delta x^2} \right] + \left[\frac{T_{i,j-1}^n - 2 \cdot T_{i,j}^n + T_{i,j+1}^n}{\Delta y^2} \right] \right) \quad (23)$$

Introducing $d = \frac{\kappa \cdot \Delta t}{\rho c \cdot \Delta x^2}$ which can be seen as a parameter to regulate the numerical stiffness and considering $\Delta x = \Delta y$ for simplicity, equation 23 becomes:

$$T_{i,j}^{n+1} = T_{i,j}^n + d \cdot \left(T_{i-1,j}^n + T_{i+1,j}^n - 4 \cdot T_{i,j}^n + T_{i,j-1}^n + T_{i,j+1}^n \right) \quad (24)$$

where,

- i: represents the node location along the x-direction.
- j: represents the node location along the y-direction.
- n: represents the time steps.
- Δx : represents the length of the grid ($= K$).
- Δy : represents the width of the grid ($= L$).

*Note: For simulation, $\Delta x = \Delta y$ is not considered and the complete equation 23 is used.

After having the simulations running, different approximations for K and L are applied. If one sets small numbers for K and L , the simulation results show smaller sampled areas covered with the actual results than larger numbers of K and L as shown in Fig. 3.1a. In our experiments, it is realised that a reasonable simulation result with $K = 21$ and $L = 31$ can be obtained (see Fig. 3.1b), as it covers the plate with the simulation results better than shown in Fig. 3.1c (measured by the areas of the plate covered with the yellow colourmap) and it is not expensive for the computational simulations.

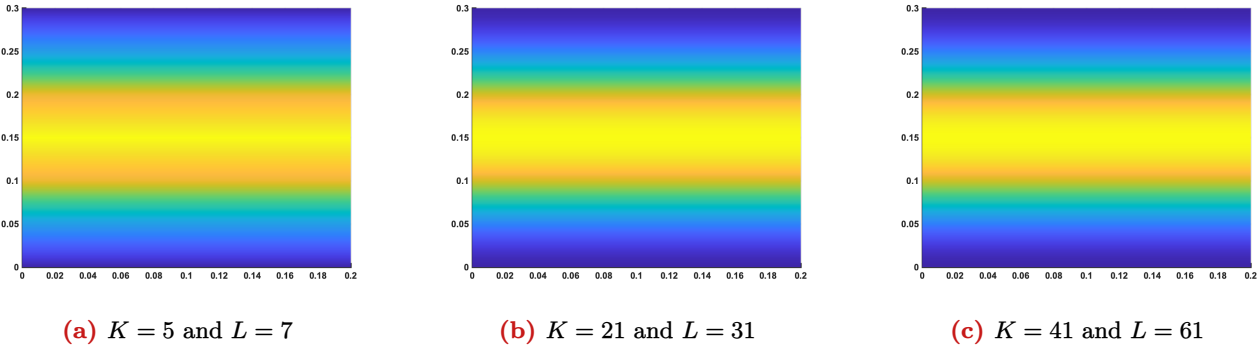


Figure 3.1: Experiments with different K and L

In order to analyse the temperature behaviour of the system with different initial temperature profiles, we set our experiment by taking the T_{amb} as the T_0 . For the corresponding orthonormal basis, the derived expressions from previous exercise is used which is as following:

$$T_0(x, y) = T_{\text{amb}} + \sum_{i=1}^K \sum_{j=1}^L \varphi_{ij}(x, y) = T_{\text{amb}} + \sum_{i=1}^K \sum_{j=1}^L \sin\left(\frac{\pi i x}{\ell_x}\right) \sin\left(\frac{\pi j y}{\ell_y}\right) \quad (25)$$

Note that the functions were changed due to the centre-weighted effect. Since one should start the experiment from the centre of the plate, one should shift the x and y to the centre. This effects the initial function from cosine and $\frac{\pi}{2}$ shift into the cosine function implies that the function becomes sine. Hence, one can arrive to the expression stated in Eq. 25. Another interesting choice for T_0 is to choose Gaussian (un-normalised) Normal function as the orthonormal basis $\varphi_{ij}(x, y) = \mathcal{N}(x, 1)\mathcal{N}(y, 1)$, in which resulting to another smooth solution.

From Fig. 3.2a, it is clear that the solution respects the boundary conditions. The difference of the T_0 choice become hard to differentiate if one opted the Gaussian initial conditions (as shown in Fig. 3.2b) as the solution is comparable between each others. The only difference is the heat diffusivity converges faster for the sine functions (35.3887°C) than in the Gaussian initial condition (35.8456°C) to the T_{amb} for the same amount of time taken into the simulation.

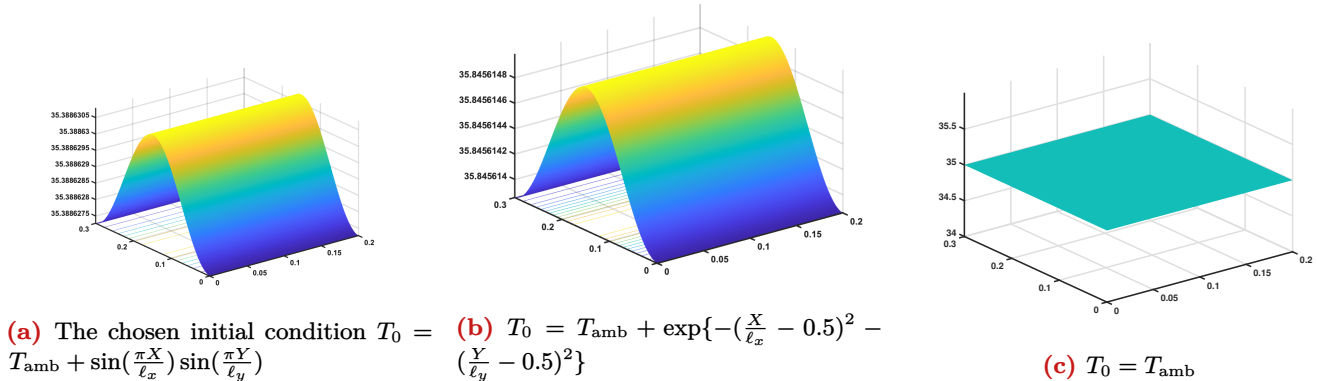


Figure 3.2: Experiments with different initial conditions

Another experiment was conducted by applying an identical temperature T_{amb} all across the plate. In this simulation, one can say that it almost certainly doesn't show any dynamics. Furthermore, this initial profile posed a numerical stiffness problem, which therefore should be disregarded for further experiments.

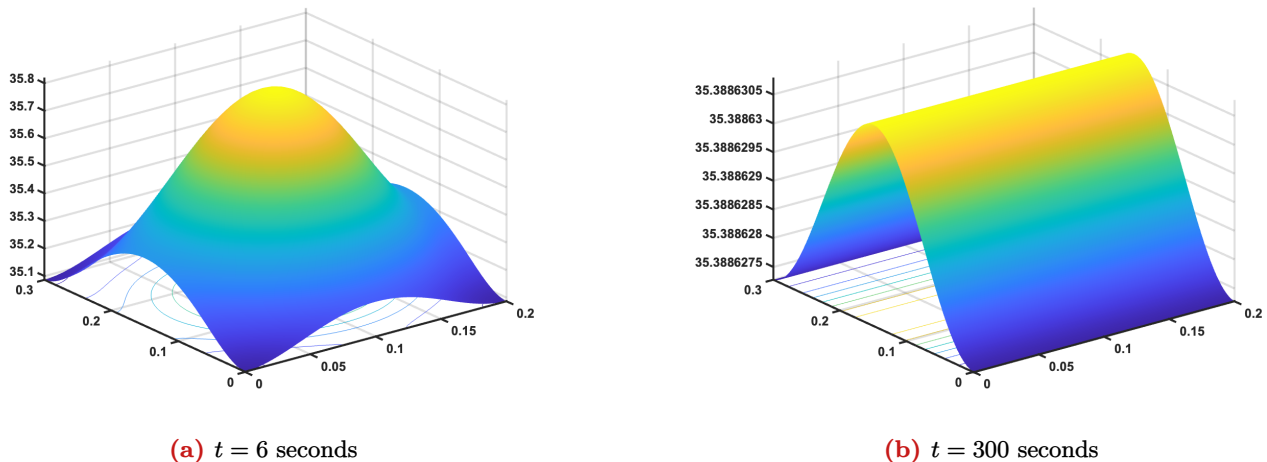


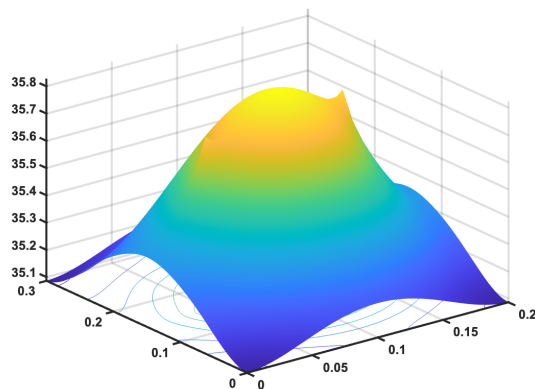
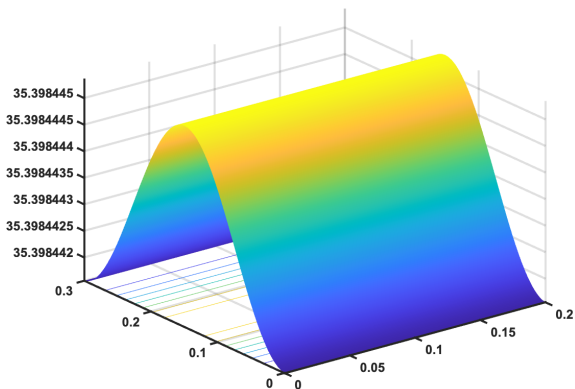
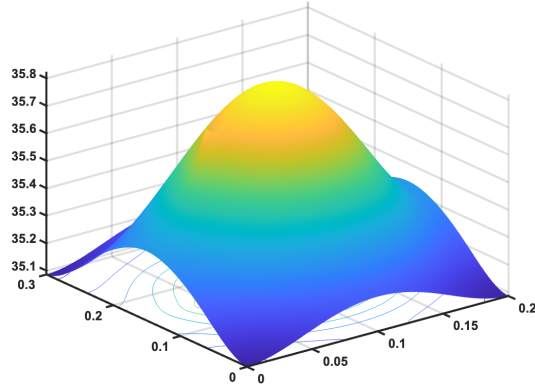
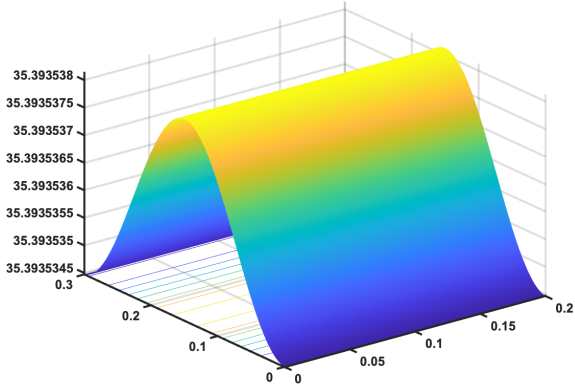
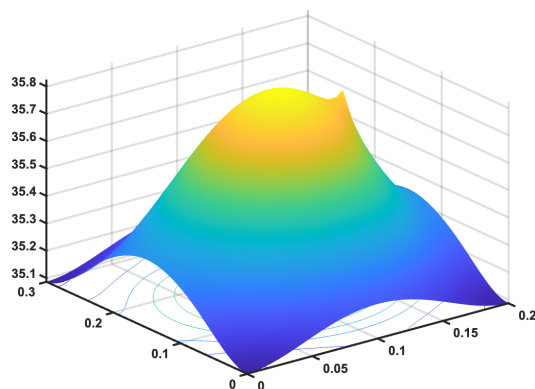
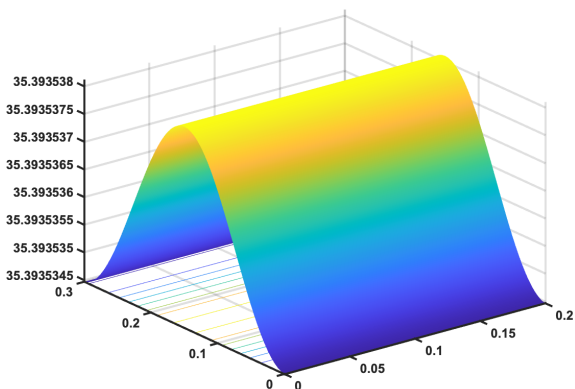
Figure 3.3: Experiment without input source

Since in all previous experiments there were no inputs applied, a realistic and time-varying inputs for the heat fluxes $u_1(t)$ and $u_2(t)$ can be chosen as a discontinuous function. In a realistic setting, an industrial grade laser as an input has a heat flux of $2000 \text{ [kW/m}^2]$. Realistic duration of this application takes typically 10 seconds.

$$u(t) = \begin{cases} 2000000, & 0 \leq t \leq 10 \\ 0 & \text{otherwise} \end{cases} \quad (26)$$

The input function is indeed realistic, as most of the input source has uniform distribution. Furthermore, it is also how it is applied in real settings, where a laser is pointed for maximal 10 seconds on the top of a plate and the number is based on the tolerance of most industrial heat flux sensors. Applying the expression in Eq. 26, $K = 21$, $L = 31$, and the chosen initial condition, the simulation result is shown in Fig. 3.4. For the applied heat sources (e.g.: $u_1(t)$ and $u_2(t)$) at $t = 6$ seconds, there are temperature spikes as shown in Fig. 3.4a and the shape of the solution at $t = 300$ seconds is similar to the one without given any inputs (shown in Fig. 3.3b).

Similarly, for one applied heat source at $t = 6$ seconds, there is a temperature spike as shown in Fig. 3.5a and Fig. 3.6a for only $u_1(t)$ and $u_2(t)$ respectively. Interestingly, both of the simulations that only given one heat source converges to the same steady state, as shown in Fig. 3.5b or Fig. 3.6b.

(a) $t = 6$ seconds(b) $t = 300$ seconds**Figure 3.4:** Experiment with 2 input sources $u_1(t)$ and $u_2(t)$ (a) $t = 6$ seconds(b) $t = 300$ seconds**Figure 3.5:** Experiment with an input source $u_1(t)$ (a) $t = 6$ seconds(b) $t = 300$ seconds**Figure 3.6:** Experiment with an input source $u_2(t)$

3.5 | Question 7 & 8

In order to produce a good quality Proper Orthogonal Decomposition (POD) model reduction, one must have enough data (also known as snapshots). For this experiment, one can take $K = 41$, $L = 61$, initial condition as mentioned in Eq. 25, and inputs $u_1(t)$ and $u_2(t)$ as introduced in Eq. 26. Furthermore, taking longer time ($t = 600$ seconds instead of 300 seconds as previously used in section 3.4) provides more data to perform a POD both qualitative and quantitative. In this experiment, one can implement the direct POD method after generating the data [1].

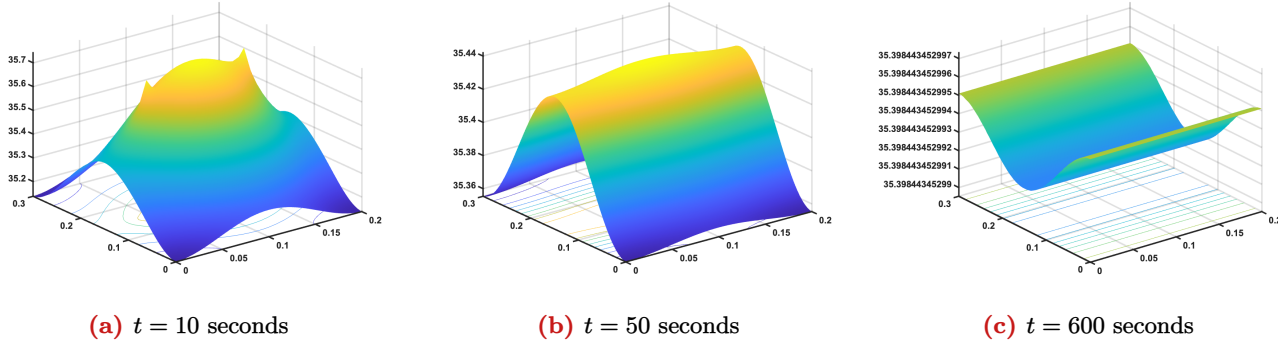


Figure 3.7: Real model simulation

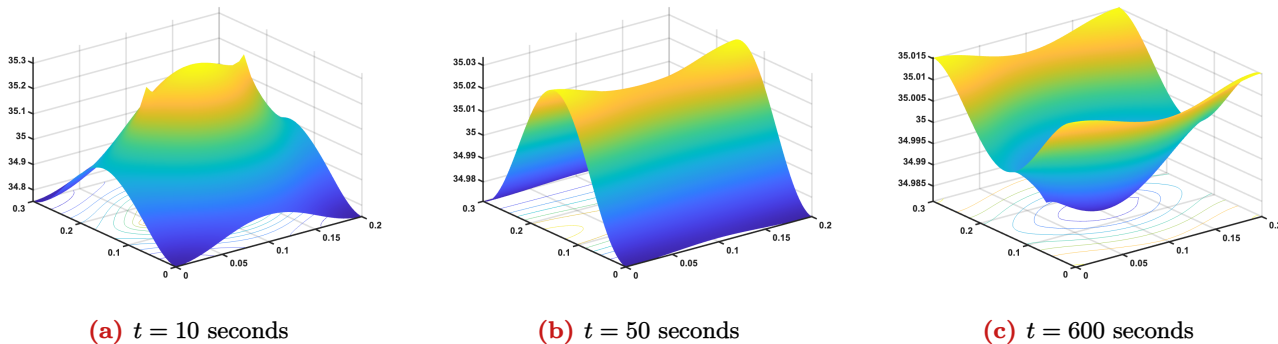


Figure 3.8: POD reduced model simulation of order $R = 5$

The POD reduced model of order $R = 5$ (as shown in Fig. 3.8) shows good representation of what is happening while the inputs contributes to the heat of certain area of plate. Compared to the real model simulation (as shown in Fig. 3.7), both of them are almost identical at $t = 10$ seconds with the real model simulation. A noticeable difference can be found at $t = 600$ seconds, where the plate's temperature shown in Fig. 3.8c doesn't match exactly as the real model simulation in Fig. 3.7c. Furthermore, some simulations regarding to this matter had been conducted by changing the temperature initial profiles, time ranges, and both the K and L . The results of those were the same, but those will get worse when K and L are lowered down. A suspicion might be that there are some numerical stiffness involved during the simulation, which occurs around $t = 50$ seconds (shown in Fig. 3.8b. For other experimentation, the quality of POD will be elaborated thoroughly in Section 3.6.

3.6 | Question 9

To check whether one have already the perfect order of POD, one should take a look at the singular values. From Fig. 3.9a, it is clear that the POD simulation conducted in Section 3.5 has recover of approximate 99.08% of the total energy from the real model as the reduction order $R = 5$.

Choosing higher R order means that one should get better results and worse otherwise. However, if one compare the $R = 3$ results in Fig. 3.10 with the $R = 5$ results in Fig. 3.8, there is only one noticeable difference in Fig. 3.10a, in which the temperature spikes at the heat sources' locations are less pronounced compared to Fig. 3.8a at $t = 10$ seconds. Similarly, the $R = 7$ results in Fig. 3.11a is more pronounced, as one take higher approximation order of POD model. The same phenomena as previous experiment for 5th-order POD happens from $t = 50$ seconds (shown in Fig. 3.10b, 3.8b, and 3.11b for $R = 3$, $R = 5$ and $R = 7$ respectively) and the real model (in Fig. 3.7b). This phenomena goes up until the end time $t = 600$ seconds as shown in Fig. 3.10c, 3.8c, and 3.11c for $R = 3$, $R = 5$ and $R = 7$ respectively in comparison with the real simulation in Fig. 3.7c.

Comparing the POD results with the same approximation order between the Gaussian (in Fig. 3.13) and the sines

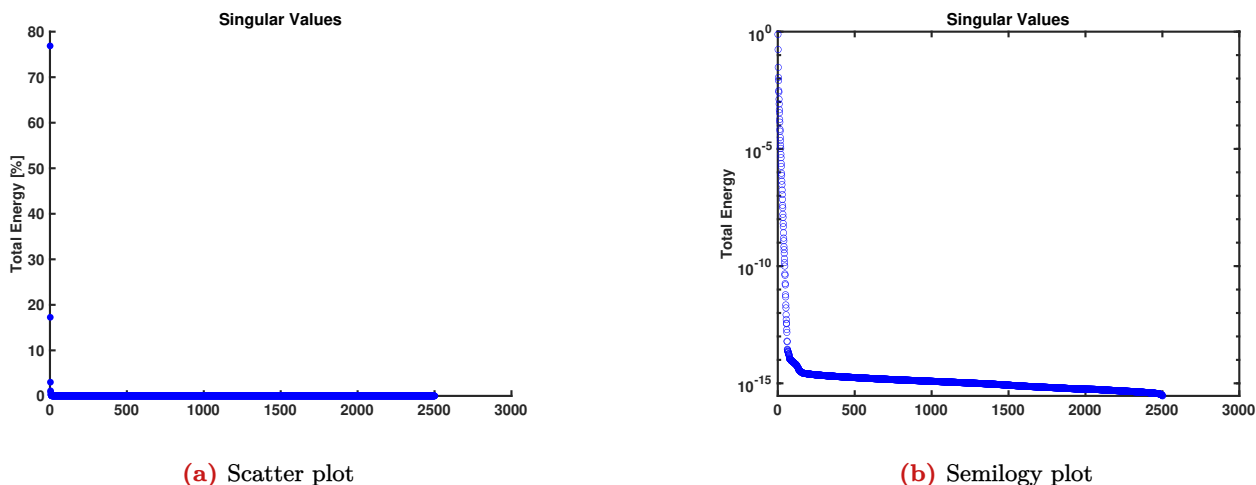


Figure 3.9: Singular values of the simulation in Section 3.5

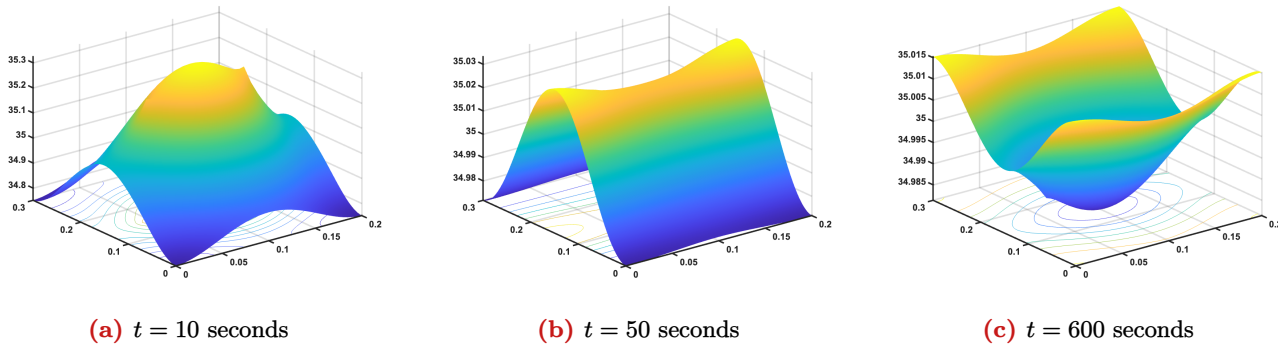


Figure 3.10: POD reduced model of order $R = 3$

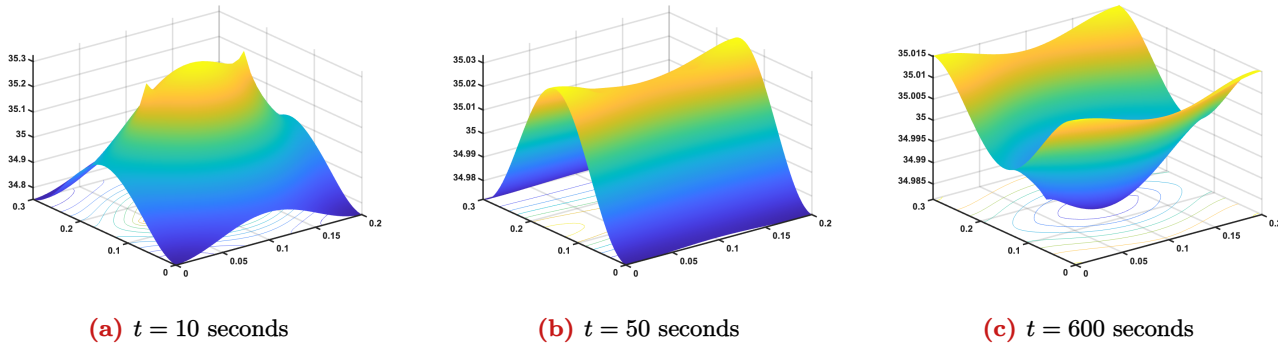


Figure 3.11: POD reduced model of order $R = 7$

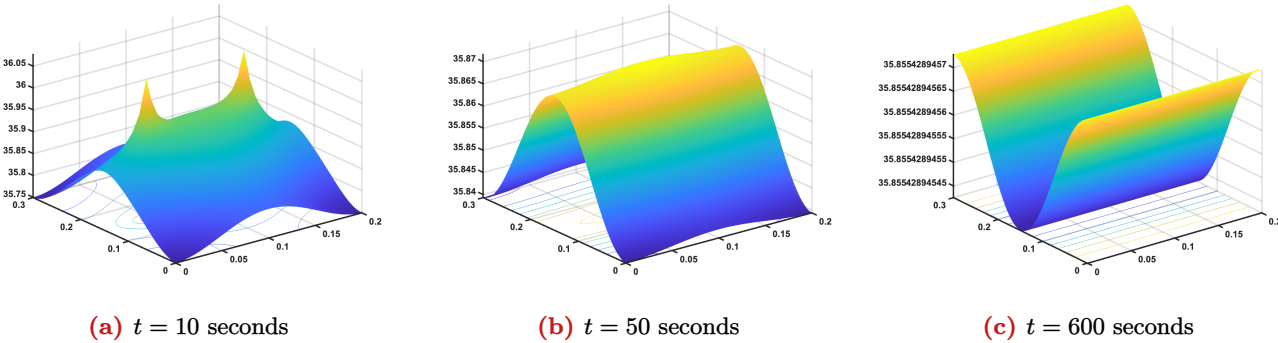


Figure 3.12: Real model with Gaussian initial profile

(in Fig. 3.8), the inputs are more pronounced at $t = 10$ seconds for the POD with Gaussian initial profiles (in Fig. 3.13a) compared to the sine functions (in Fig. 3.8a). The same occurrence keeps happening at $t = 50$ seconds (in Fig. 3.13b) and at $t = 600$ seconds, there are slight difference between POD with Gaussian initial profile and sine initial profiles, as there are a little small downward spikes for POD with Gaussian (shown in Fig. 3.13c) compared to the one with sine initial profile (shown in Fig. 3.8c).

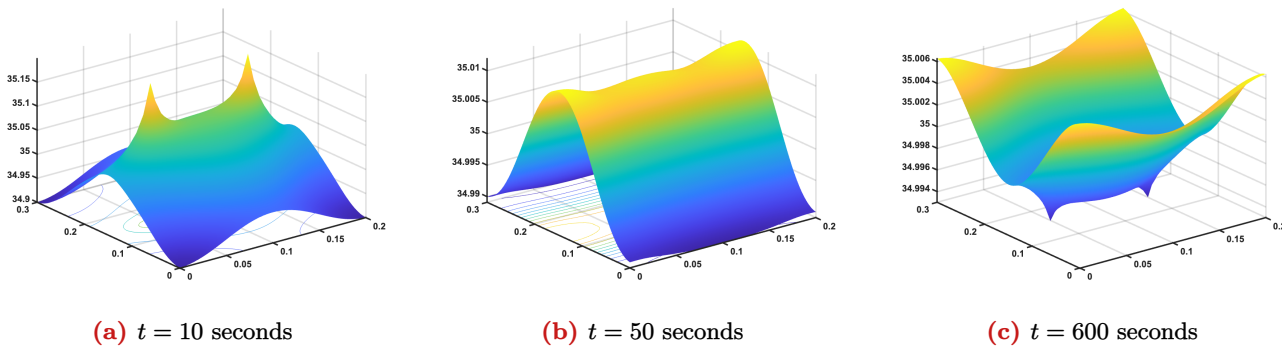


Figure 3.13: POD reduced model of order $R = 5$ with Gaussian initial profile

The effects of different inputs applied towards the POD model can be observed by giving only an input to either side of the plate. Since there are always 2 inputs applied in previous experiments, one can use only one of the input and see if there is a difference (shown in Fig. 3.15 for the POD of 5th-order and Fig. 3.14 for the real model simulation), which there is almost no difference between both of the models, except at $t = 50$ seconds, where the phenomena happened, which inverted the temperature of the plate at $t = 600$ seconds. In a conclusion, it can be

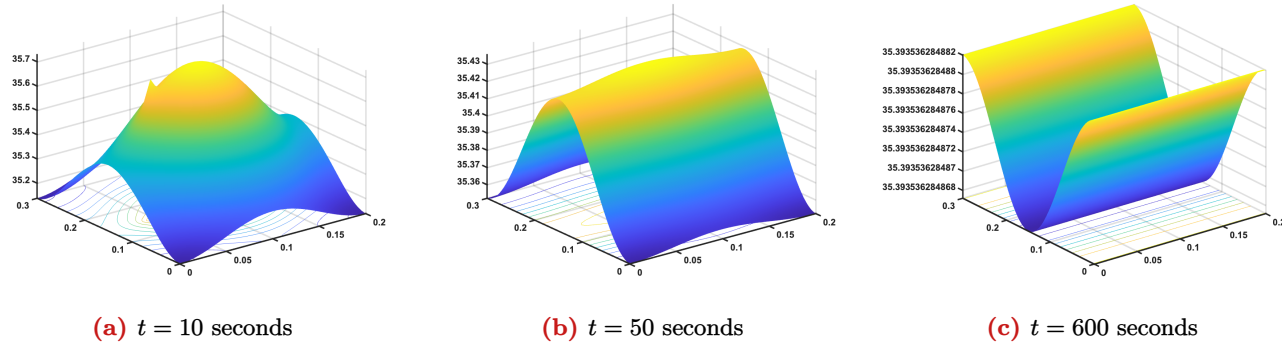


Figure 3.14: Real model with with only $u_1(t)$ applied

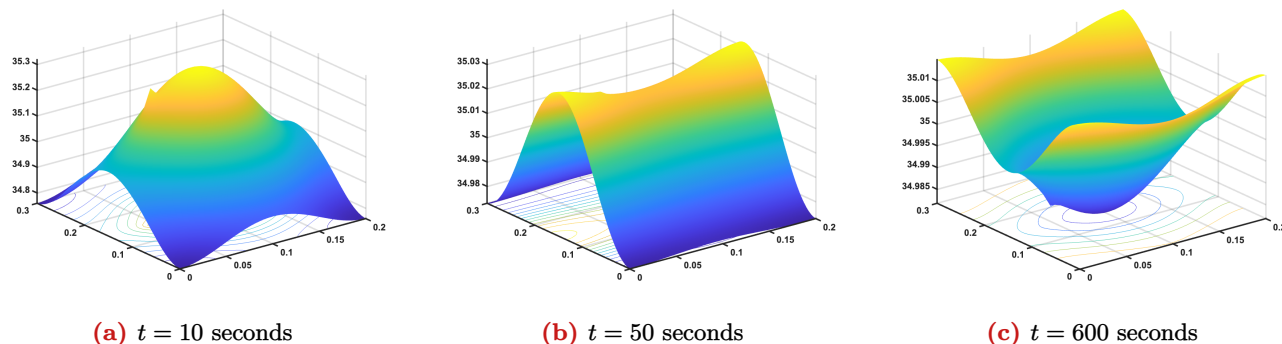


Figure 3.15: POD reduced model of order $R = 5$ with only $u_1(t)$ applied

concluded that POD approximations of 5th-order is a good model approximation of the real dynamics. Even though there are several parts that involves numerical stiffness and interesting phenomena, all of the simulation results can describe the dynamics (almost) perfectly. A new finding in the simulation is that the Gaussian initial profile simulation shows that it is manageable to be an alternative for POD, as it leads to the same "inverted temperature" phenomena and have a nice convergence too at the end. Different input selections doesn't give any better results as the simulation may involve numerical stiffness even without any input administered in the simulations.

4 | The non-homogeneous model

4.1 | Question 10

To approach this problem, with the given ℓ_x and ℓ_y values for the blue area, one can define a matrix $\alpha(x, y) := \frac{\kappa(x, y)}{\rho(x, y)c(x, y)}$ which has different numbers across the $\alpha \in \mathbb{R}^{L \times K}$. Assuming this as a constant matrix, the non-homogeneous problem can be then seen as a homogeneous problem with different constants acting on the spatial derivative of the temperature. The approximate (discrete) plot of $\alpha(x, y)$ is shown in Fig. 4.1, where the shown yellow area is actually the blue area defined in the project description and the shown blue area is the yellow area.

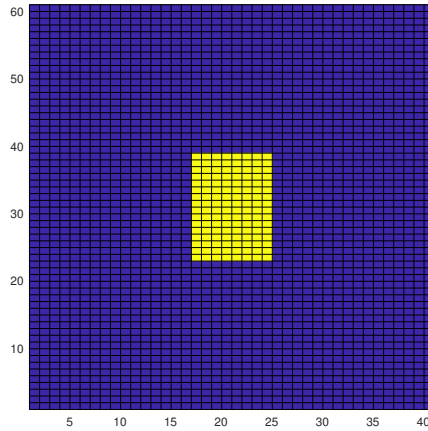


Figure 4.1: Discretised grid for $\alpha(x, y)$

After obtaining the $\alpha(x, y)$ matrix values, one can then perform the simulation with settings as in the previous experiments, with sine initial profile as mentioned in Eq. 25, $K = 41$ and $L = 61$ for simulating the POD, and 2 inputs acting on the plate as defined in Eq. 26. With all being said, the simulation results are shown in Fig. 4.2 and 4.3 for the real model and POD of 5th-order reduced model respectively.

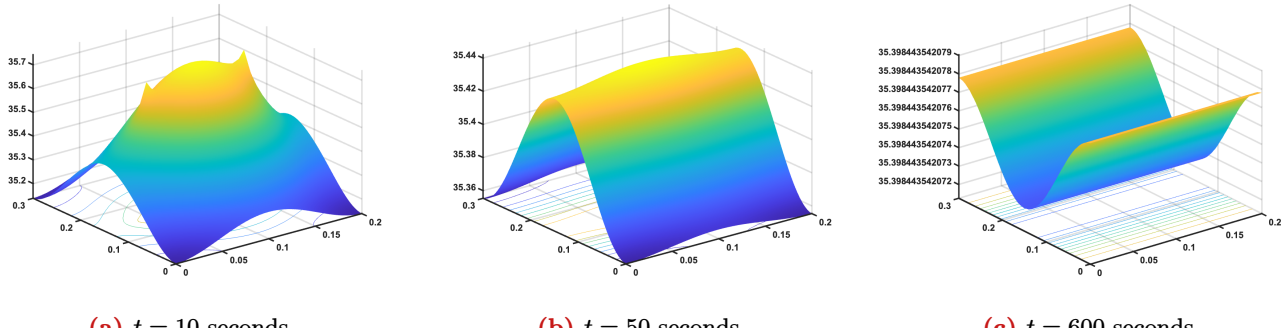


Figure 4.2: Non-homogeneous real model simulation

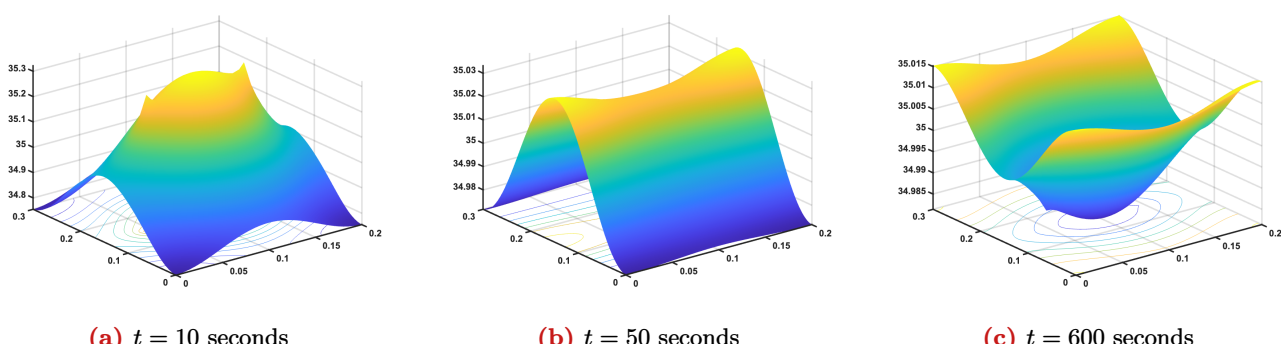


Figure 4.3: Non-homogeneous POD reduced model of order $R = 5$

5 | References

- [1] J. Weiss, “A tutorial on the proper orthogonal decomposition,” in *AIAA Aviation 2019 Forum*, 2019.